



Large magnetocaloric effect in $\text{La}_{0.75}\text{Ca}_{0.25-x}\text{Na}_x\text{MnO}_3$ ($0 \leq x \leq 0.10$) manganites

Souhir Bouzidi^{1,2} · Mohamed Amara Gdaiem¹ · S. Rebaoui³ · J. Dhahri¹ · E. K. Hlil⁴

Received: 24 September 2019 / Accepted: 6 December 2019 / Published online: 1 January 2020
© Springer-Verlag GmbH Germany, part of Springer Nature 2020

Abstract

We have studied the effect of a partial substitution of Ca^{2+} by Na^+ on the structural, magnetic and magnetocaloric properties of the mixed valence perovskites $\text{La}_{0.75}\text{Ca}_{0.25-x}\text{Na}_x\text{MnO}_3$ ($0 \leq x \leq 0.10$), prepared by the flux method. X-ray diffraction studies revealed that our samples crystallize in the orthorhombic structure with a Pbnm space group. Rietveld analysis showed that MnO_6 octahedron has a little distortion and that $\theta_{\text{Mn-O-Mn}}$ bond angles increase with increasing Na^+ content. The field cooled (FC) and zero field cooled (ZFC) magnetizations indicated that our samples have a paramagnetic-ferromagnetic phase transition, when decreasing temperature. A small deviation was observed between FC and ZFC curves. This deviation can be explained by the competition between the ferromagnetic and antiferromagnetic interactions, leading to a glassy behavior. The Curie temperature, T_C , increased from 268 K for $x=0$ to 278 K for $x=0.10$. The magnetizations isotherms of our compounds, with a second-order phase transition, were investigated. For the $x=0.10$ sample, the maximum of the magnetic entropy change was found to be 3.15 and 6.44 $\text{J kg}^{-1} \text{K}^{-1}$, under an applied magnetic field of 2 and 5 T, respectively. Moreover, it has important relative cooling power values of about 134.82 and 317.79 J kg^{-1} , under the same applied magnetic field. In addition, rescaled entropy data collapsed into the same curve, which indicates the universal behavior for the magnetocaloric effect (MCE) in our compounds. These materials could be potential candidates as working substances in magnetic refrigeration.

1 Introduction

In the recent years, synthesis of magnetic materials as a thin films and nanostructures has been investigated for various applications due to their unique structural, electrical and magnetic properties [1-3]. Perovskite manganites with the general formula $\text{Ln}_{1-x}\text{MMnO}_3$ (where Ln is a trivalent rare earth ion and M is a divalent ion such as alkaline elements)

have been widely studied during the last few years. This is due to their important physical properties such as colossal magnetoresistance (CMR), metal-insulator transition, and charge/orbital ordering. These properties make perovskite manganites as the potential candidates especially for the refrigeration technology [4-10]. Furthermore, these materials have many advantages such as their small volume requirement, chemical stability, low production cost, and high efficiency. Indeed, they are environment friendly, which makes them very attractive to further scientific research. Currently, there are other materials belonging to the family of oxides, which have attracted the attention of researchers, they are more suitable for future technological domains such as ferrites with the structure of perovskite, spinel, and magnetoplumbite [11, 12]. We can mention that the hexaferrites are the strongest magnetic compounds with $T_C \sim 740$ K. This is the simplest type of all ferrites with a hexagonal structure. More than 90% of permanent magnets are produced all over the world based on these compounds. They have a ferromagnetic structure and a total magnetic moment of 20 μB in the ground state. Moreover, the resonant frequency is determined by the frequency of natural ferromagnetic resonance.

✉ Mohamed Amara Gdaiem
gdaiem_mohamed@hotmail.fr

¹ Laboratoire de la Matière Condensée et des Nanosciences, Département de Physique, Faculté des Sciences de Monastir, Avenue de l'Environnement Monastir, 5019 Monastir, Tunisia

² Higher School of Science and Technology of Hammam Sousse, University of Sousse, Sousse, Tunisia

³ Laboratory of Physics of Materials and Nanomaterials Applied at Environment, Faculty of Sciences in Gabes, Gabes University, Gabes, Tunisia

⁴ Institut Néel, CNRS et Université Joseph Fourier, BP 166, 38042 Grenoble Cedex 9, France

In addition, hexaferrites are physiologically harmless [13, 14]. In other hand, some works have been focused on the oxygen deficiency effect in manganites system, as important parameters that affect the magnetic properties. The oxygen non stoichiometry is very important for complex transition oxides and changes seriously the total magnetic moment and Curie point. It leads to the formation of a weak magnetic state such as spin glass and change some magnetic parameters [15–17].

The parent compound, LaMnO_3 , is an antiferromagnetic (AFM) insulator, in which only Mn^{3+} ions are present. It is characterized by a super exchange (SE) coupling between Mn^{3+} sites. Upon the substitution of a divalent ion (M), in the Ln site, a few Mn^{3+} with the electronic configuration $(3d^4, t_{2g}^3 \uparrow e_g^1 \uparrow, S = 2)$ transform into Mn^{4+} ions with the electronic configuration $(3d^3, t_{2g}^3 \uparrow e_g^0, S = 3/2)$. During this transformation, the e_g electron becomes delocalized. The holes facilitate the charge transfer in the e_g band, which is highly hybridized with the oxygen $2p$ state. According to Hund's rule, the charge transfer induces a ferromagnetic (FM) coupling between Mn^{3+} and Mn^{4+} ions. This coupling gives rise to a double-exchange transfer (DE) of spin-polarized electrons from Mn^{3+} to Mn^{4+} ions [18]. Generally, the substitution in Ln-sites controls the $\text{Mn}^{3+}/\text{Mn}^{4+}$ ratio in this type of material. In particular, Lanthanum manganites have attracted the attention of several researchers, thanks to the very rich phase diagram observed in $\text{La}_{1-x}\text{Ca}_x\text{MnO}_3$ and $\text{La}_{1-x}\text{Sr}_x\text{MnO}_3$ samples. Lanthanum manganites are characterized by multi-phase transitions, including: paramagnetic (PM)—insulator, PM—metallic, FM—insulator, FM—metallic, AFM—metallic, spin canted—insulator, charge-ordered, and canted AFM states, together with different variations of the critical temperatures [19–21].

Furthermore, upon the addition of Na to the LaMnO_3 sample, an amount ($2x$) of Mn^{3+} transform into Mn^{4+} . Taking charge neutrality into account, the chemical formula can be defined as: $\text{La}_{1-x}^{3+}\text{Na}_x^+(\text{Mn}_{1-2x}^{3+}\text{Mn}_{2x}^{4+})\text{O}_3$. As a first interpretation, the substitution of La by a small amount of Na results in a large number of charge carriers, leading to an increase in the conductivity. In addition, the potential between the Na and the La ions increases although the ionic radii of La^{3+} and Na^+ are comparable. This is due to the large valence difference between them. The study of the effect of the substitution of Na on lanthanum manganite may provide a better understanding of the CMR effect in these materials [22, 23]. There are several works that are interested on the divalent ions substituted manganites such as [24–27]. They are focused on the studying of structural, magnetic, and electrical properties of perovskite materials, especially after the creation of oxygen vacancies.

Among the different studied manganites, $\text{La}_{0.75}\text{Ca}_{0.25}\text{MnO}_3$ sample has attracted exceptional interest in several recent works. This is due to its good physical properties. Yi et al. observed that the MR of $\text{La}_{0.75}\text{Ca}_{0.25}\text{MnO}_3$ sample is strengthened at low temperatures. This is due to the spin-polarized tunneling phenomena [28]. In addition, Pekala et al. observed that MR does not tend to zero at low temperatures, which confirms that grains size is fine [29]. Moreover, Guo et al. noted that this sample admits a large magnetic entropy change [30]. Thus, $\text{La}_{0.75}\text{Ca}_{0.25}\text{MnO}_3$ is one of the most widely studied manganite systems.

As a contribution to the investigation of manganite materials, we report here the study of the effect of Na substitution on the structural and magnetic properties and MCE effect of $\text{La}_{0.75}\text{Ca}_{0.25}\text{MnO}_3$ samples. There are several synthesis methods of magnetic materials, the usual methods such as sol–gel and solid-state reactions or the new process such as sol–gel auto combustion technique [31] and the citrate sol–gel method [32]. In our work, we choose to prepare our samples by flux method using sodium chloride (NaCl) as a flux.

In our work, we choose to prepare our samples by flux method using sodium chloride (NaCl) as a flux.

The advantages of NaCl solvents are the presence of a common anion and the insignificant incorporation of Na into the material to be synthesized at low temperature, which prevents the evaporation of Na. In our previous work [33], we detected the high doping effect of Na content on $\text{La}_{0.75}\text{Ca}_{0.25}\text{MnO}_3$ sample. In our present paper, we choose to test the low Na content effect and to compare it with our last results.

2 Experimental details

To produce a very high quality, homogenous, and nano-poly-crystalline powder, $\text{La}_{0.75}\text{Ca}_{0.25-x}\text{Na}_x\text{MnO}_3$ ($0 \leq x \leq 0.10$) compounds were prepared by the flux method, using NaCl as a flux. All experimental details are stated in our last work [33]. The structure and phase purity of the prepared sample were determined by powder X-ray diffraction (XRD) at room temperature using a Panalytical X pert Pro-diffractometer with Cu-K_α radiation ($\lambda = 1.5406 \text{ \AA}$). Data for Rietveld refinement were collected in a 2θ range between 10° and 100° with a scanning step of 0.017 and a time step of 18 s . The structural analyses were carried out by the Rietveld method using the FULLPROF program [34]. The micro-structure was studied by a scanning electron microscope (SEM) at room temperature using a Philips XL30. In addition, a semi-quantitative analysis was performed at 20 kV accelerating voltage using energy dispersive X-ray analyses (EDX).

Magnetizations (M) as a function of temperatures (T) were performed using an extraction magnetometer developed in Louis Neel Laboratory of Grenoble. Magnetization isotherms (M ($\mu_0 H$)) were measured in the range of 0–5 T fields, for different temperatures, around Curie temperature (T_C). M ($\mu_0 H$) measurements were corrected by a demagnetization factor, noted D , obtained from M ($\mu_0 H$) curves at low-fields linear response at a low-temperature region.

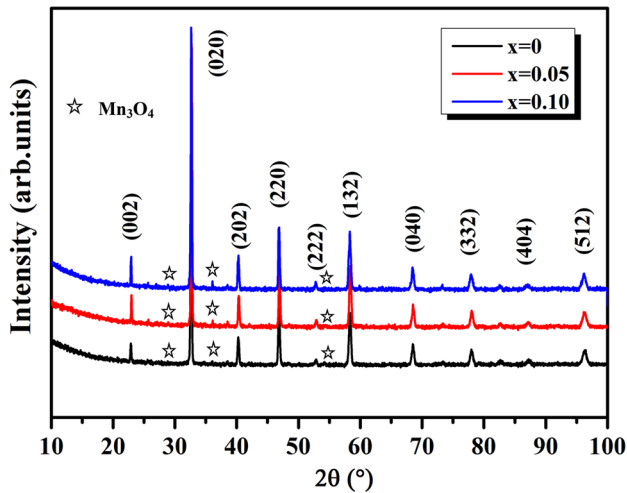


Fig. 1 XRD pattern of $\text{La}_{0.75}\text{Ca}_{0.25-x}\text{Na}_x\text{MnO}_3$ ($0 \leq x \leq 0.10$) samples at room temperature

3 Results and discussions

3.1 X-ray diffraction study

As a first step, we carried out XRD analysis to verify the crystal structure of the studied samples. Powder XRD patterns of $\text{La}_{0.75}\text{Ca}_{0.25-x}\text{Na}_x\text{MnO}_3$ ($0 \leq x \leq 0.10$) compounds, collected at room temperature, are plotted in Fig. 1. We note that our samples are of a single phase with a very small amount of Mn_3O_4 , as found in recent works [33]. XRD data were carried out using Rietveld refinement [35]. Figure 2 exemplifies the Rietveld refinement of XRD profile for $\text{La}_{0.75}\text{Ca}_{0.20}\text{Na}_{0.05}\text{MnO}_3$ sample, with good agreement between the observed and the calculated profiles. This is due to the excellent goodness of χ^2 . The analyzed data showed that our samples crystallize in the orthorhombic structure with Pbnm ($Z=4$) space group no (62), in which the (La/Ca/Na) is at 4 (c) ($x, y, 1/4$) position, (Mn) at 4 (b) ($1/2, 0, 0$), O_1 at 4 (c) ($x, y, 1/4$), and O_2 at 8 (d) (x, y, z). On the other hand, in our previous work [33] for $x=0.15$ and 0.20 , we found that the $x=0.15$ sample is a mixture of orthorhombic and rhombohedral structures with Pbnm and $\text{R}\bar{3}\text{c}$ space groups, respectively. While, the $x=0.20$ sample is characterized by the rhombohedral structure with a $\text{R}\bar{3}\text{c}$ space group. We can remark that for the low doping rate, we can get the same space group (for $x=0, 0.05$ and 0.1), followed by a change of crystallographic structure with the increase of doping rate (in the case of our previous work).

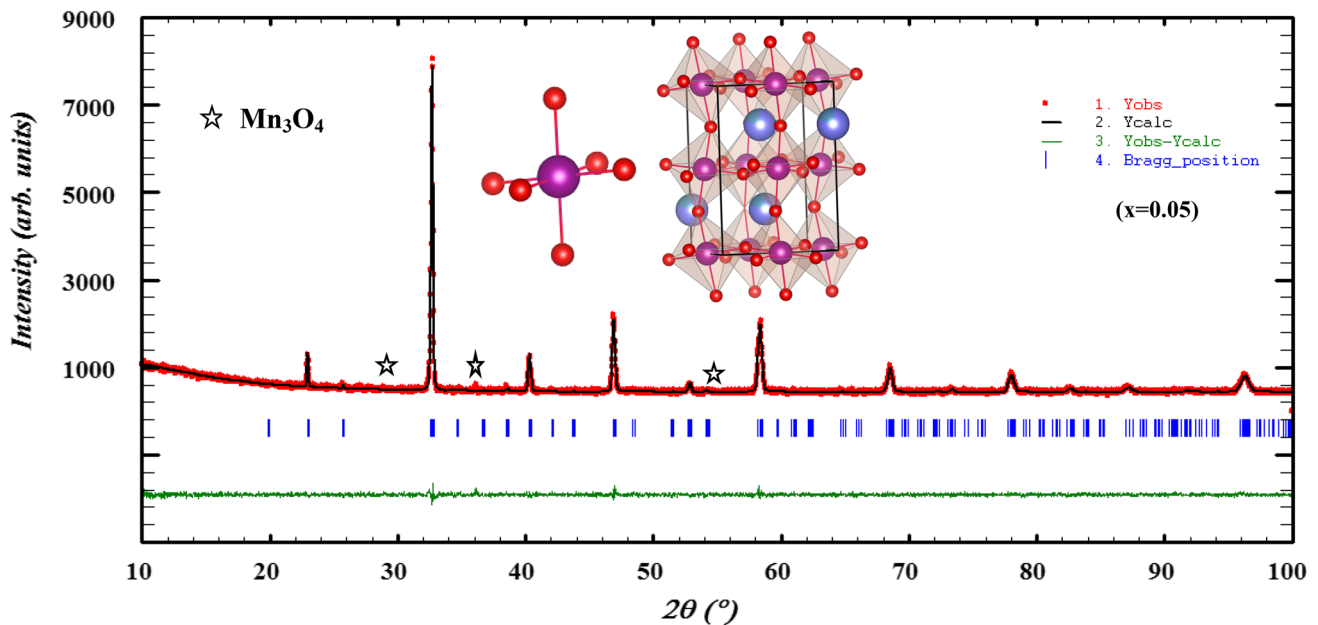


Fig. 2 The observed and calculated solid line of XRD patterns of $\text{La}_{0.75}\text{Ca}_{0.20}\text{Na}_{0.05}\text{MnO}_3$ sample determined by Rietveld refinement. The vertical lines show the Bragg's peak positions and the lowest

curve shows the difference between the data and the calculation patterns. The inset shows the crystal structure of $\text{La}_{0.75}\text{Ca}_{0.20}\text{Na}_{0.05}\text{MnO}_3$

The unit cell and different fitting parameters of our samples are summarized in Table 1.

The relative amount of Mn_3O_4 was determined from XRD patterns of the samples by measuring the relative intensities of the major $\text{La}_{0.75}\text{Ca}_{0.25-x}\text{Na}_x\text{MnO}_3$ ($0 \leq x \leq 0.10$) and Mn_3O_4 peaks, using the following expression [36, 37]:

$$\text{Mn}_3\text{O}_4(\%) = 100 \times \frac{I_{\text{Mn}_3\text{O}_4}}{I_{\text{Mn}_3\text{O}_4} + I_{\text{Pbnnm}}}, \quad (1)$$

where $I_{\text{Mn}_3\text{O}_4}$ is the major Mn_3O_4 peak and I_{Pbnnm} is the major $\text{La}_{0.75}\text{Ca}_{0.25-x}\text{Na}_x\text{MnO}_3$ ($0 \leq x \leq 0.10$) peak. We found that the relative impurity amount of Mn_3O_4 is negligible and does not affect the physical properties.

Lattice distortions may be caused by Jahn–Teller effect inherent to the Mn^{3+} high spin state or the connecting pattern of MnO_6 octahedron leading to the formation of rhombohedral or orthorhombic lattice. Furthermore, the tolerance

factor, T_G , is introduced to describe the ionic match between A and B site ions and to predict the distortion of the perovskite structure. This is defined by the following expression [38, 39]:

$$T_G = \frac{\langle r_{(\text{La,Ca,Na})} \rangle + \langle r_{\text{O}} \rangle}{\sqrt{2}(\langle r_{\text{Mn}} \rangle + \langle r_{\text{O}} \rangle)}. \quad (2)$$

The manganese oxide compounds have a perovskite structure if their T_G is in the range of $0.89 < T_G < 1.02$ [40]. The obtained values of T_G for our samples are listed in Table 1. This confirms the stability of this structure.

From Table 1, we can remark that the unit cell volume increases with the increase in Na content. According to Shannon [41], the ionic radius of ($r_{\text{Na}^+} = 1.24 \text{ \AA}$) is higher than that of ($r_{\text{Ca}^{2+}} = 1.18 \text{ \AA}$). On the other hand, the average of ($r_{\text{Mn}^{3+}} = 0.645 \text{ \AA}$) is larger than that of ($r_{\text{Mn}^{4+}} = 0.53 \text{ \AA}$). Generally, the bigger ion at the substituted site can strengthen some Mn–O–Mn bond angle, which results in the decrease of the average Mn–O bond distance. This hypothesis was confirmed by the determination of Mn–O–Mn angles and Mn–O distances, using the Rietveld refinement (Table 1). It has been reported that the deformation of the MnO_6 octahedron may be responsible for the distortion in the perovskite structures. The crystal structure and MnO_6 octahedron of the sample ($x = 0.05$) were drawn using VESTA program [42] based on the refined atomic positions (shown in the inset of Fig. 2).

Table 1 Refined structural parameters determined from X-ray Rietveld refinement for $\text{La}_{0.75}\text{Ca}_{0.25-x}\text{Na}_x\text{MnO}_3$ ($0 \leq x \leq 0.10$) samples measured at room temperature

	$x=0$	$x=0.05$	$x=0.10$
a (Å)	5.474 (2)	5.492 (6)	5.499 (1)
b (Å)	5.465 (8)	5.468 (9)	5.471 (1)
c (Å)	7.736 (6)	7.733 (5)	7.737 (2)
V (Å ³)	231.494	232.309	232.776
La/Ca/Na			
x	0.500 (7)	0.498 (6)	0.496 (8)
y	0.017 (1)	0.014 (9)	0.012 (9)
B_{iso} (Å ²)	1.12 (4)	1.09 (1)	1.11 (3)
Mn			
B_{iso} (Å ²)	0.64 (1)	0.65 (3)	0.71 (5)
O_1			
x	0.557 (7)	0.574 (7)	0.563 (9)
y	0.496 (2)	0.482 (4)	0.477 (2)
B_{iso} (Å ²)	1.42 (1)	1.49 (6)	1.51 (3)
O_2			
x	0.181 (3)	0.236 (8)	0.221 (1)
y	0.308 (1)	0.272 (7)	0.283 (6)
z	0.024 (8)	0.034 (6)	0.025 (1)
B_{iso} (Å ²)	1.59 (2)	1.61 (5)	1.57 (1)
Discrepancy factors			
R_p (%)	3.80	3.54	3.71
R_{wp} (%)	4.77	4.50	4.71
χ^2	1.18	1.11	1.23
Bond lengths and bond angles			
$\langle \theta_{\text{Mn-O-Mn}} \rangle$ (°)	155.15	158.82	159.91
$\langle d_{\text{Mn-O}} \rangle$ (Å)	1.99 (3)	1.98 (9)	1.97 (5)
Bandwidth W (10 ⁻²) (a.u)	8.73 (8)	8.85 (5)	9.09 (4)
Tolerance factor, T_G	0.9649	0.9685	0.9721

3.2 Morphological properties

The average crystallite sizes of $\text{La}_{0.75}\text{Ca}_{0.25-x}\text{Na}_x\text{MnO}_3$ ($0 \leq x \leq 0.10$) compounds were determined using Scherrer's formula after the evaluation of the most intense peak broadening and SEM. Scherrer's formula can be written as [43]:

$$D = \frac{K\lambda}{\beta \cos(\theta)}, \quad (3)$$

where $\lambda = 1.5406 \text{ \AA}$ is the wavelength for CuK_α radiation, θ is the diffraction angle of the most intense peak, K is the shape factor equal to 0.9, β is the full width at half maximum of the highest peak. The average crystallite sizes are listed in Table 2.

The morphological properties of our samples were studied using SEM (inset of Fig. 3, for $x = 0.05$ as an example). We can notice that our samples have polycrystalline characteristics. The average particle sizes were determined by ImageJ software [44] and calculated using Gaussian functions. From Table 2, the calculated grain sizes are larger than those calculated by Scherrer's formula. This indicates that each particle is formed by several crystallites [45]. The influence of grain size on the perovskite materials has been

Table 2 Average crystallites sizes calculated by Scherrer’s formula and SEM

Samples	$x=0$	$x=0.05$	$x=0.10$
$\langle r_A \rangle$ (Å)	1.355	1.357	1.361
D_{Sch} (nm)	35	43	46
D_{SEM} (µm)	1.84	1.91	1.98

Table 3 Results of EDX analysis

Nominal composition	Typical cationic composition from EDX			
	La	Ca	Na	Mn
$\text{La}_{0.75}\text{Ca}_{0.25}\text{MnO}_3$	0.751	0.249	–	0.999
$\text{La}_{0.75}\text{Ca}_{0.20}\text{Na}_{0.05}\text{MnO}_3$	0.752	0.201	0.048	1.001
$\text{La}_{0.75}\text{Ca}_{0.15}\text{Na}_{0.10}\text{MnO}_3$	0.749	0.152	0.101	0.998

investigated by many researches. Mahesh et al. [46] have varied the grain size from 0.025 to 3.5 µm and they get a significant change in properties. They observe that when the grain size decreases, there is an enhancement in the low magnetoresistance temperature. There are many works that have been concentrated to understand the mechanism of inter-grain tunneling conduction such as Doroshev et al. [47] and Zhang et al. [48]. The average crystallite size of our samples is calculated from the XRD and SEM analyses. We can observe that the average increases as a function of Na content. In our work, we will discuss the effect of this slight grain size increase on the magnetic properties.

To check the existence of all elements in our samples, EDX was performed at room temperature. Figure 3 represents the EDX spectrum, for $x=0.05$ as an example. We can see clearly that La, Ca, Na, Mn, O elements are present, which indicates that there is no loss of any integrated element during the sintering process. The typical cationic composition for our samples is represented in Table 3.

3.3 Magnetic study

To better understand the magnetic behavior of our samples, Fig. 4 shows the temperature dependence of FC and ZFC, under an applied field of 0.05 T in the temperature range of 5–330 K. It is clearly remarkable that our samples underwent a sharp magnetic transition from FM to PM state when increasing temperature. This behavior was remarked in our last work for $x=0.15$ and 0.20 [33]. Also, we can see from this figure that the magnetization values, which were quite stable at temperatures below 230 K for $x=0$, 235 K for $x=0.05$, and 240 K for $x=0.10$ began to decrease rapidly at T_C . A small divergence between FC and ZFC curves can be observed at the irreversibility temperature of 250 K for $x=0$, 255 K for $x=0.05$, and 260 K for $x=0.10$. This phenomenon is observed in other magnetic materials [49–51], which is assigned to the existence of an isotropic field generated from FM clusters [50]. At low temperatures, a small peak was observed around 40 K. This confirms the presence of Mn_3O_4

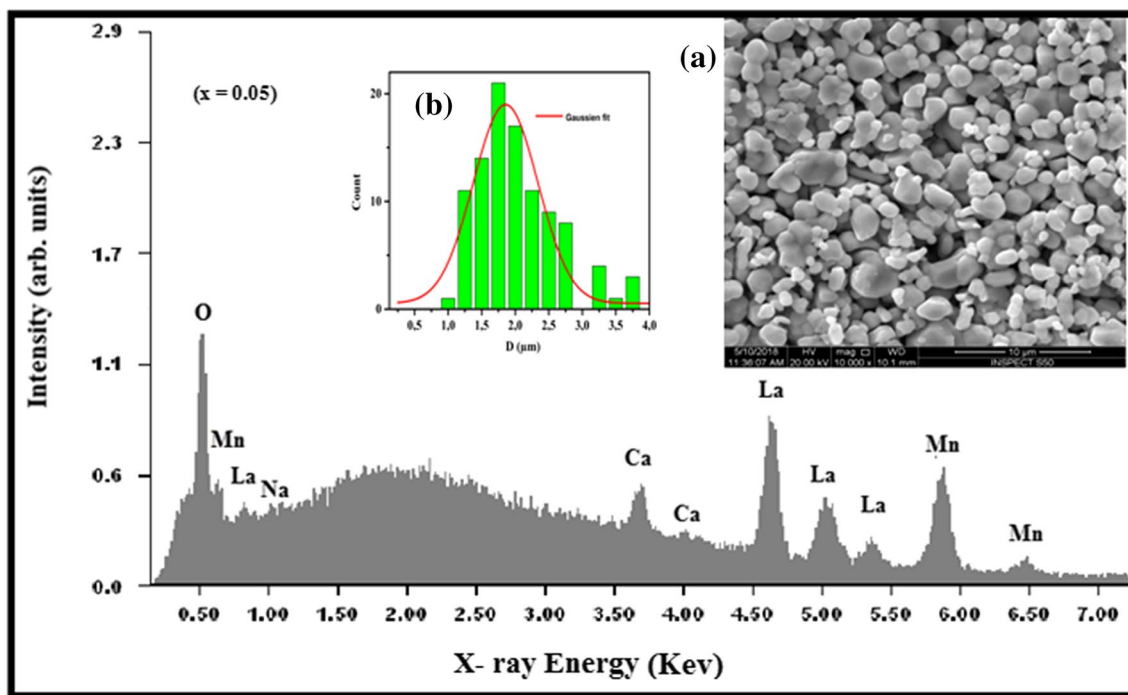


Fig. 3 EDX analysis for $x=0.05$. **a** Shows the typical SEM and **b** shows the histogram of the distribution of particles size

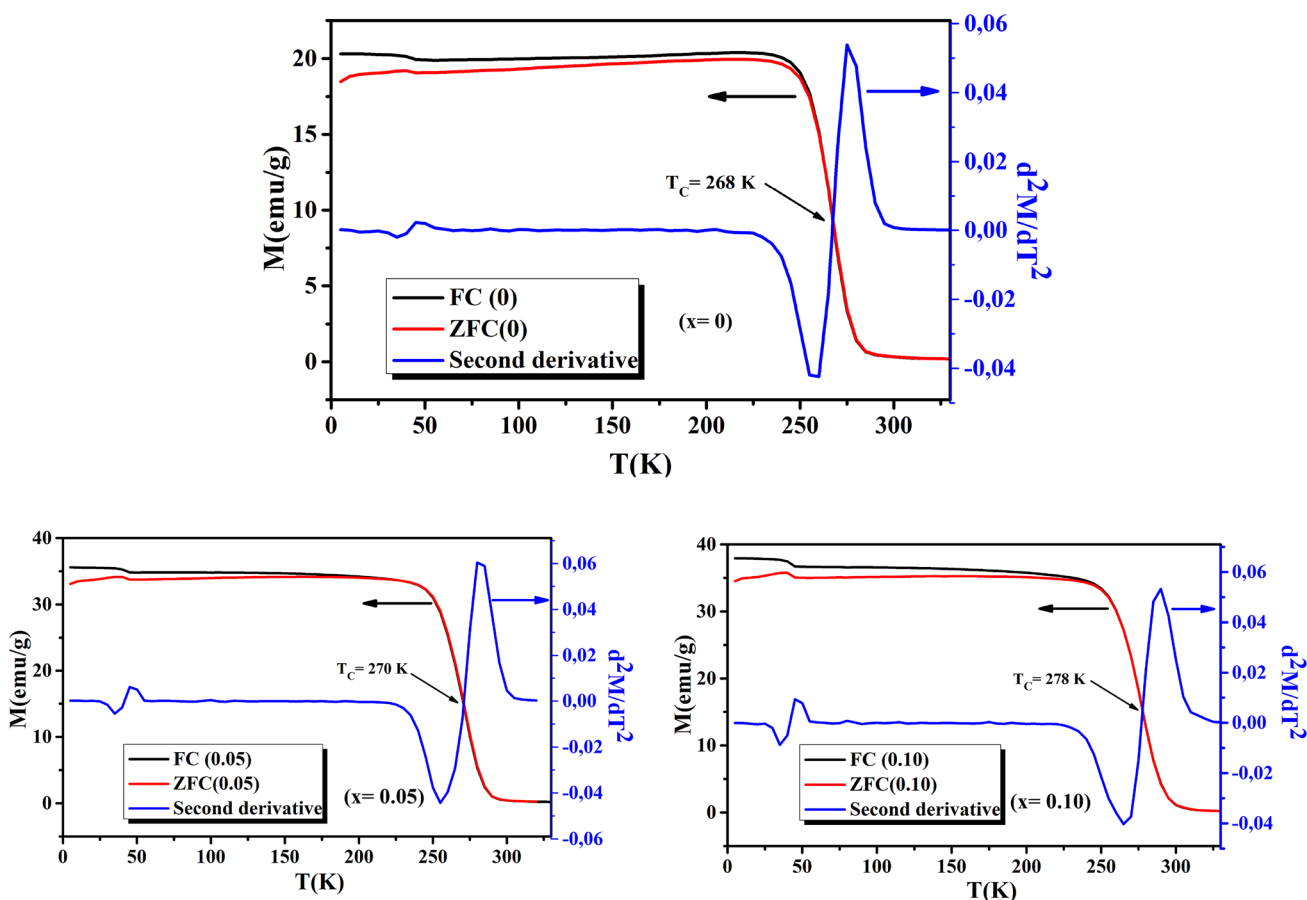


Fig. 4 The ZFC and FC magnetizations and d^2M/dT^2 as function of temperatures for $\text{La}_{0.75}\text{Ca}_{0.25-x}\text{Na}_x\text{MnO}_3$ ($0 \leq x \leq 0.10$) samples, under a magnetic field of 0.05 T

secondary phase [52, 53]. T_C was calculated from d^2M/dT^2 as a function of temperatures. From Fig. 4 (blue color), T_C values were found to be around 268, 270, and 278 K, respectively, for $x=0$, $x=0.05$, and $x=0.10$. However, for $x=0.15$ and 0.20, T_c values are equal to 301.5 and 300 k, respectively. We can conclude that when the doping rate increases, T_c approaches room temperature, which indicates that our samples are good candidates for the refrigeration domain. In our work, the substitution of Ca^{2+} by Na^+ led to an increase of the Mn^{4+} content from 25 ($x=0$) to 35% ($x=0.10$). This is explained by the increase of $\langle \text{Mn-O-Mn} \rangle$ bond angle and the decrease of $\langle \text{Mn-O} \rangle$ bond distance. Therefore, the DE interactions were gradually strengthened, which resulted in the increase of FM character. This is not the case for $x=0.15$ and 0.20 in which the increase of Mn^{4+} content above 40%, produced a decrease in the DE interaction and enhanced the SE interaction [54]. It is worth noting that all samples show a ferromagnetic behavior with close phase transition temperature. Their magnetization is strongly influenced by the grain size. It increases with the increase of grain size, which is due to the decrease of magnetically disordered states at

the surface of grains. Therefore, the increase of particle size decreases the surface to volume ratio, thereby increasing the net magnetization. This is leading to increases the ferromagnetic transition temperature. T_c passed from 268 to 278 °C for our samples.

The bandwidth is characterized by the overlap between Mn_{3d} and O_{2p} orbitals. It can be described empirically by the following expression [55]:

$$W_b \approx \frac{\cos w}{d_{(\text{Mn-O})}^{3.5}}, \tag{4}$$

where $w=1/2(\pi - \langle \text{Mn-O-Mn} \rangle)$ and $d_{(\text{Mn-O})}$ is the bond length. The calculated W_b values are tabulated in Table 1. We can remark that W_b is inversely proportional to Mn-O-Mn angle. This result is attributed to the increase of $\langle ra \rangle$. It may be explained by the increase of the average grain size. These changes lead to a significant rise in the Curie temperature [56]. In addition, the substitution of Ca^{2+} by Na^+ leads to the increase of the order effect. According to Trukhanov

et al., an average grain size is inversely related to the surface tension forces' relative to the bulk elastic forces [57].

To comprehend the dynamics of spin, we have calculated the inverse of magnetic susceptibility as a function of temperature from the magnetization data ($M(T)$). In the high-temperature range, the susceptibility obeys the Curie–Weiss (CW) law, defined by:

$$\chi = \frac{C}{T - \theta_p}, \tag{5}$$

where θ_p is the CW temperature and C is the Curie constant, defined by [58]:

$$C = \frac{N_a}{3k_B} \mu_{\text{eff}}^2, \tag{6}$$

where $N_a = 6.023 \times 10^{23} \text{ mol}^{-1}$ is the number of Avogadro and k_B is Boltzmann's constant.

The linear PM region was fitted using Eq. (5). The obtained θ_p values are listed in Table 4. Noting that θ_p value can be negative, positive, or null according to whether the behavior, respectively, is AFM, FM, or PM. The positive value of θ_p , in our case, indicates the presence of FM interactions between the spins. Also, we can note that the obtained values of θ_p are greater than those of T_C for each sample. This may be due to magnetic inhomogeneity above T_C . Thus, we have also calculated the experimental effective moment $\mu_{\text{eff}}^{\text{exp}}$ using Eq. (6) and the theoretical one ($\mu_{\text{eff}}^{\text{theo}}$) is calculated by:

$$\mu_{\text{eff}}^{\text{theo}} = \sqrt{(0.75 - x) [\mu_{\text{eff}}(\text{Mn}^{3+})]^2 + (0.25 + x) [\mu_{\text{eff}}(\text{Mn}^{4+})]^2}, \tag{7}$$

where $\mu_{\text{eff}}(\text{Mn}^{3+}) = 4.9 \mu_B$ and $\mu_{\text{eff}}(\text{Mn}^{4+}) = 3.87 \mu_B$ [59].

The different calculated $\mu_{\text{eff}}^{\text{exp}}$ and $\mu_{\text{eff}}^{\text{theo}}$ values are listed in Table 4. We can remark a difference between these two parameters. This may be attributed to FM correlations in PM region, which is probably caused by the formation of FM clusters [60]. Our results are comparable to those obtained in the literature [60, 61]. It is important to mention that the paramagnetic moment and the susceptibility (M/H) can be seen to be decreasing with the increase in the crystallite size. To better understand the magnetic properties of our samples,

Table 4 Some experimental values for $\text{La}_{0.75}\text{Ca}_{0.25-x}\text{Na}_x\text{MnO}_3$ ($0 \leq x \leq 0.10$) samples

	$x=0$	$x=0.05$	$x=0.10$
T_C (K)	268	270	278
θ_p (K)	269	277	284
$\mu_{\text{eff}}^{\text{theo}}$ (μ_B)	4.66 (2)	4.61 (3)	4.56 (1)
$\mu_{\text{eff}}^{\text{exp}}$ (μ_B)	6.40 (6)	6.25 (4)	6.13 (2)

the hysteresis cycles $M(\mu_0H)$, at low temperature, were studied. Figure 5a, b displays $M(\mu_0H)$ at 10 K of the range of $\mu_0H = \pm 6$ T, for $x=0.00$ and 0.10 samples, as examples. From these figures, we can see a similar behavior with a small hysteresis loop. The insets of Fig. 5a, b display a zoomed portion of the low magnetic field region. We can see clearly that magnetization increased rapidly at a low applied field. Surprisingly, a sharp saturation was observed in which the M_S values were found to be 92.65 and $105.43 \text{ emu g}^{-1}$ for $x=0.00$ and 0.10 , respectively. This indicates the typical FM behavior. Additionally, we remarked that our samples have negligible values of the remnant magnetizations (M_r) and the coercive fields (μ_0H_C). μ_0H_C values were found to be 52×10^{-4} and 19×10^{-4} T, for $x=0.00$ and 0.10 , respectively. M_r values were found to be 2.30 and 1.40 emu g^{-1} for $x=0.00$ and 0.10 , respectively. These three parameters change slightly with change in the grain size. The increase of the grain size led to the decreases of the total grain boundary

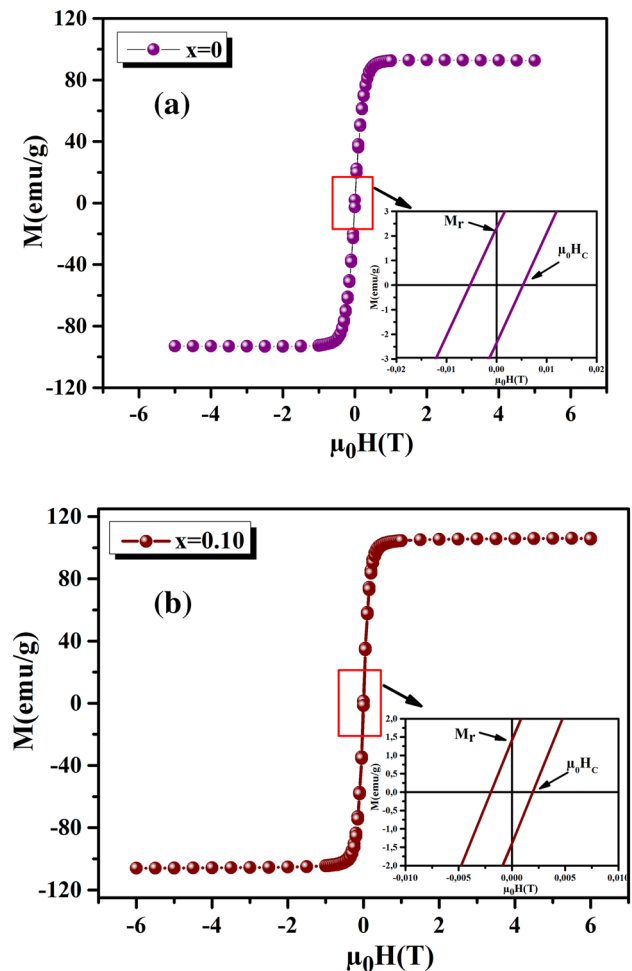


Fig. 5 Magnetic hysteresis cycles at $T=10$ K of $\text{La}_{0.75}\text{Ca}_{0.25-x}\text{Na}_x\text{MnO}_3$ ($0 \leq x \leq 0.10$) samples. The insets show a zoom portion of the low magnetic field region

and therefore, the movement of domains becomes easier inside the crystal leading to increase in M_s and decrease in H_C . Here, we can conclude that our samples have a soft FM behavior. These results make them good candidates for some technological applications such as reading and writing process in high density recording media or information storage [62]. In addition, $x=0.15$ and 0.20 [33], have also negligible values. In which, M_S values were found to be 88.10 and 92.21 emu g⁻¹, μ_0H_C values were found to be 21×10^{-4} and 16×10^{-4} T, and M_r values were equal to 1.49 and 1.11 emu g⁻¹, for $x=0.15$ and $x=0.20$, respectively. Together with hysteresis loop studies, we measured magnetization as a function of the applied magnetic field around their FM–PM phase transition, as shown in the inset of Fig. 6 for our studied samples. At the low temperature region, we can see a rapid increase in the magnetization at the weak magnetic field region up to 1 T. Then, $M(\mu_0H)$ curves reached saturation as a result of increase in the magnetic field, indicating a typical FM state. This is caused by the complete alignment of the spins in our studied samples.

To get a deeper understanding of the nature of the magnetic phase transition for our samples, we derived the Arrott’s plots (M^2 vs. μ_0H/M) from $M(\mu_0H)$ (Fig. 6). According to Banerjee’s criterion [63, 64], if the slope of the curve is negative, the magnetic transition is of first order. Otherwise, it is of second order, which is the case in our study.

3.4 Magnetocaloric study

Magnetocaloric effect is an intrinsic property of magnetic materials. It represents their thermal response under the application or elimination of an external magnetic field. The coupling between the lattice and spin plays an important role, which leads to an additional magnetic entropy change near T_C and favors MCE. $-\Delta S_M$ allows one to verify whether a magnetic material may be considered as a good magnetic refrigerant or not. It can be calculated from the isothermal magnetization curves under different magnetic fields. According to the fundamentals of thermodynamics, $-\Delta S_M$ produced by the variation of the applied magnetic field from 0 to μ_0H_{max} , can be expressed by the following expression [65]:

$$\Delta S_M(T, \mu_0H) = S_M(T, \mu_0H) - S_M(T, 0) = \int_0^{\mu_0H_{max}} \left(\frac{\partial S}{\partial(\mu_0H)} \right)_T d(\mu_0H). \tag{8}$$

From Maxwell’s thermodynamics, a relationship between $-\Delta S_M$ and M is defined as:

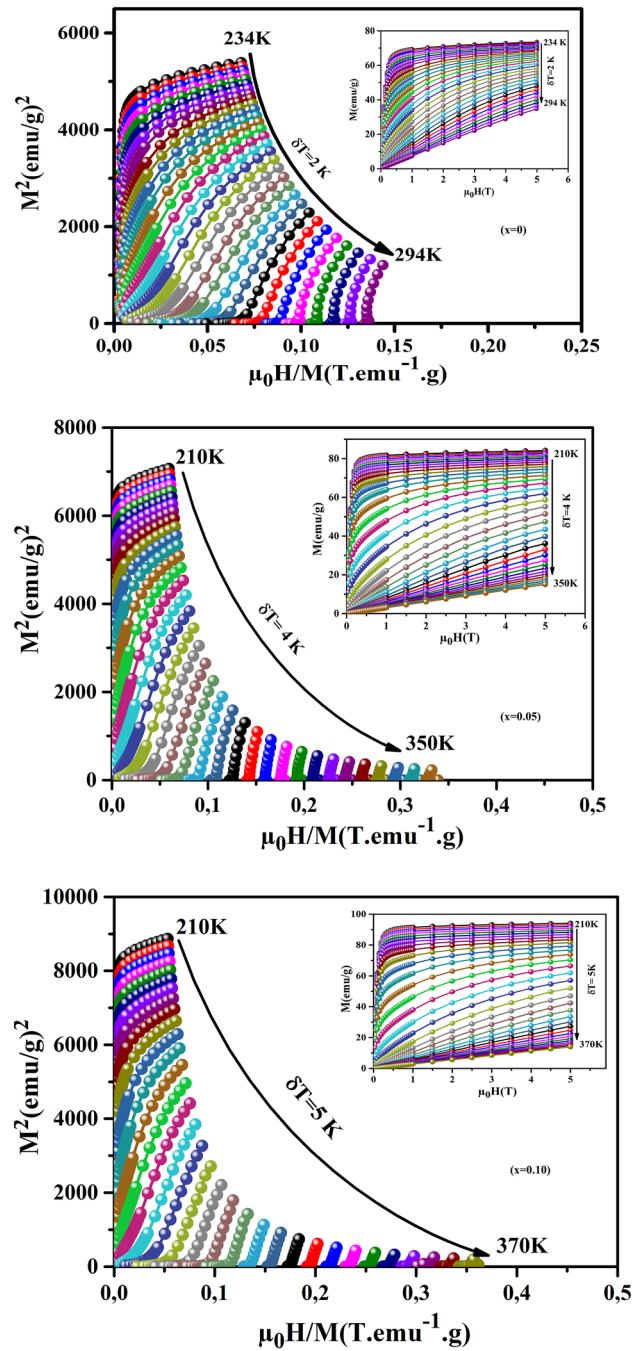


Fig. 6 M^2 vs. μ_0H/M plots, for $La_{0.75}Ca_{0.25-x}Na_xMnO_3$ ($0 \leq x \leq 0.10$) samples. Insets show $M(\mu_0H)$ curves at different temperatures

$$\left(\frac{\partial S}{\partial(\mu_0H)} \right)_T = \left(\frac{\partial M}{\partial T} \right)_{(\mu_0H)}. \tag{9}$$

Then, one can determine the following relation:

$$\Delta S_M(T, \mu_0 H) = \int_0^{\mu_0 H_{\max}} \left(\frac{\partial M}{\partial T} \right)_{\mu_0 H} d(\mu_0 H). \tag{10}$$

Here $\mu_0 H_{\max}$ represents the maximum of the applied magnetic field [66].

Generally, to predict MCE, $-\Delta S_M$ is often determined by some different numerical calculations. The first approximation is a direct method, based on the $M(T)$ measurement under different external magnetic fields. In the case of a small discrete field, $-\Delta S_M$ can be approximated as [67]:

$$\Delta S_M \left(\frac{T_1 + T_2}{2} \right) = \frac{1}{T_2 - T_1} \left[\int_0^{\mu_0 H_{\max}} M(T_2, \mu_0 H) d(\mu_0 H) - \int_0^{\mu_0 H_{\max}} M(T_1, \mu_0 H) d(\mu_0 H) \right]. \tag{11}$$

The second one is based on $M(\mu_0 H)$ measurement. To evaluate $-\Delta S_M$, one needs to use a numerical approximation to the integral in Eq. (9). $-\Delta S_M$ can be written as [68]:

$$-\Delta S_M(T, \Delta(\mu_0 H)) = \sum \frac{M_{i+1}(T_{i+1}, \mu_0 H_{i+1}) - M_i(T_i, \mu_0 H_i)}{T_{i+1} - T_i} \Delta \mu_0 H_i, \tag{12}$$

M_i and M_{i+1} are the experimental magnetization values, respectively, at T_i and T_{i+1} , under an external magnetic field $\mu_0 H_i$ [69].

In the following part of this work, we have used the first approximation to evaluate the variation of $-\Delta S_M$ as a function of temperature under an applied magnetic field. Figure 7 displays $-\Delta S_M(T)$ for our samples. The obtained curves are similar to those obtained in other perovskite manganites [70, 71]. They have a positive sign in all studied temperatures, which confirms the FM behavior. Our studied samples exhibit $-\Delta S_M^{\max}$ of 6.25, 6.35, and 6.44 $\text{J kg}^{-1} \text{K}$ at a magnetic field of 5 T for $x=0, 0.05$, and 0.10, respectively. On other hand, $x=0.20$ sample exhibited a classical behavior of $-\Delta S_M$ with $-\Delta S_M^{\max}$ equal to 6.01 $\text{J kg}^{-1} \text{K}^{-1}$. While, $x=0.15$ indicated the coexistence of two peaks, which corresponds to two-Curie temperatures [33]. We can notice also, that for low Na content our samples $x=0, 0.05$, and 0.10 exhibited high entropy values, better than $x=0.15$ and 0.20. Here, it is important to mention that the magnetic entropy change was observed to increase with increase in the magnetic field and to be higher for the high grain size.

In magnetic refrigeration, another useful parameter to quantify the efficiency of MC material is the relative cooling power (RCP). This latter refers to the heat transfer between the hot and cold reservoirs in the ideal refrigeration cycle. This parameter represents the area under $-\Delta S_M(T)$ curve. It is defined as [72-74]:

$$\text{RCP} = -\Delta S_M^{\max}(T, \mu_0 H) \times \delta T_{\text{FWHM}}, \tag{13}$$

where, δT_{FWHM} is the full width at half maximum in $-\Delta S_M(T)$ curve.

Figure 8 shows the variation of δT_{FWHM} and RCP as a function of the applied magnetic field at T_C for $x=0.10$ as an example. A monotonous increase is seen in these parameters when increasing the applied magnetic field. This increase is due to the weakness of the effect of spin coupling that is less important when the applied magnetic field is high. Table 5 presents the obtained $-\Delta S_M^{\max}$ and RCP values for our samples together with those obtained in other magnetic materials. From this table, it is clear that our values are in agreement with those obtained in the literature. This makes our compounds potential candidates for magnetic refrigeration.

The magnetization related change of the specific heat, $\Delta C_{p, \mu_0 H}$, is expressed as:

$$\Delta C_p(T, \mu_0 H) = C_p(T, \mu_0 H) - C_p(T, 0) = T \frac{\partial \Delta S_M(T, \mu_0 H)}{\partial T}. \tag{14}$$

Using this equation, we calculated $\Delta C_{p, \mu_0 H}$ as a function of temperature for our samples under different applied magnetic fields (Fig. 9). We can see that $\Delta C_{p, \mu_0 H}$ changed sharply around T_C , from a negative to a positive value, upon increasing temperatures [75, 76]. The sum of the two parts is the magnetic contribution to the total specific heat. This affects the heating or cooling power of magnetic refrigerators. $\Delta C_{p, \mu_0 H}$ data of a magnetic material are useful in the design of a refrigerator.

To get better insights into MCE, Amaral [77, 78] proposed a theatrical modeling based on Landau's theory of magnetic phase transition. Gibbs free energy can be developed as follows [77]:

$$G(T, M) = G_0 + \frac{1}{2}A(T)M^2 + \frac{1}{4}B(T)M^4 + \frac{1}{6}C(T)M^6 + \dots - \mu_0 HM, \tag{15}$$

where $A(T)$, $B(T)$, and $C(T)$ are temperature-dependent parameters according to the thermal variation of the amplitude of the spin fluctuation known as Landau's coefficients.

In the equilibrium condition, $\partial G / \partial M = 0$, the magnetic equation of state is derived as:

$$\frac{\mu_0 H}{M} = A(T) + B(T)M^2 + C(T)M^4. \tag{16}$$

Fitting Arrot's plots by the last equation, the evolution of the best obtained values of Landau's coefficients as function temperatures is shown in Fig. 10, for $x=0$, under an applied field of 5 T as an example. According to Amaral et al. [77, 79], the nature of $B(T)$ plays a fundamental role in investigating $-\Delta S_M(T, \mu_0 H)$. The inset of Fig. 10 indicates that $B(T)$ is negative below T_C . However, it has a positive sign

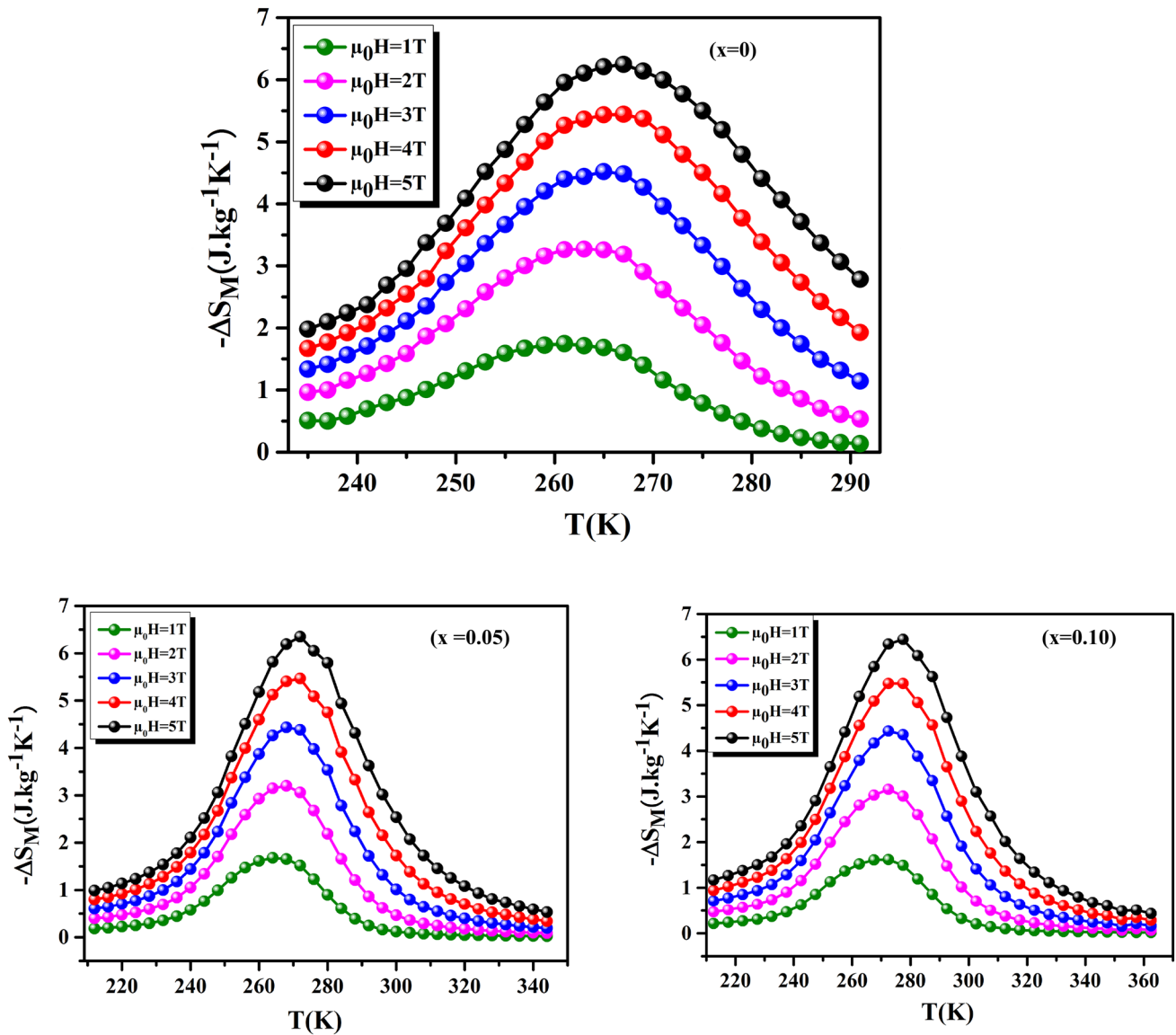


Fig. 7 $-\Delta S_M$ as function of temperatures at different magnetic fields, for $La_{0.75}Ca_{0.25-x}Na_xMnO_3$ ($0 \leq x \leq 0.10$) samples

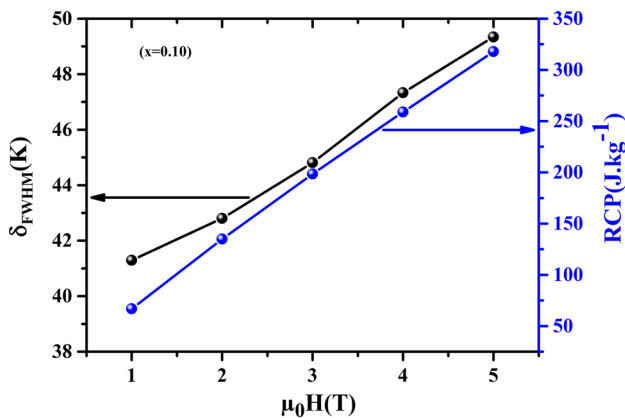


Fig. 8 RCP and δ_{FWHM} values vs. μ_0H , for $x=0.10$ sample

above T_C . The behavior of this curve is obtained in recent works [80, 81]. This suggests the second-order phase transition in our samples [82]. Therefore, using the differentiation of Gibbs free energy with respect to temperatures, we can determine $-\Delta S_M(T, \mu_0H)$ theoretically by:

$$\begin{aligned}
 S_M(T, \mu_0H) &= - \left(\frac{\partial G(\mu_0H, T)}{\partial T} \right)_{\mu_0H} \\
 &= - \frac{1}{2} \frac{\partial A}{\partial T} M^2 - \frac{1}{4} \frac{\partial B}{\partial T} M^4 - \frac{1}{6} \frac{\partial C}{\partial T} M^6.
 \end{aligned}
 \tag{17}$$

The theoretical $-\Delta S_M(T, \mu_0H)$ is defined as:

Table 5 Summary of MC properties of $\text{La}_{0.75}\text{Ca}_{0.25-x}\text{Na}_x\text{MnO}_3$ ($0 \leq x \leq 0.10$) samples compared with other magnetic materials

Samples	T_C (K)	$\mu_0 H$ (T)	$(-\Delta S_M^{\max})$ ($\text{J kg}^{-1} \text{K}$)	RCP (J kg^{-1})	References
$\text{La}_{0.75}\text{Ca}_{0.25}\text{MnO}_3$	268	5	6.25	198	Present work
$\text{La}_{0.75}\text{Ca}_{0.2}\text{Na}_{0.05}\text{MnO}_3$	270	5	6.35	270.5	Present work
$\text{La}_{0.75}\text{Ca}_{0.15}\text{Na}_{0.10}\text{MnO}_3$	278	5	6.44	317.7	Present work
$\text{La}_{0.7}\text{Ca}_{0.3}\text{MnO}_3$	227	5	6.42	–	[71]
$\text{La}_{0.67}\text{Ba}_{0.33}\text{MnO}_3$	292	5	1.48	161	[72]
$\text{La}_{0.70}\text{Sr}_{0.3}\text{Mn}_{0.9}\text{Al}_{0.1}\text{O}_3$	310	5	2.6	109	[73]
$\text{La}_{0.8}\text{Ba}_{0.2}\text{MnO}_3$	295	5	4.5	130	[74]
$\text{La}_{0.8}\text{Ba}_{0.2}\text{Mn}_{0.9}\text{Fe}_{0.1}\text{O}_3$	193	5	2.62	211	[74]
$\text{La}_{0.7}\text{Sr}_{0.3}\text{Mn}_{0.93}\text{Fe}_{0.07}\text{O}_3$	296	5	4	255	[91]

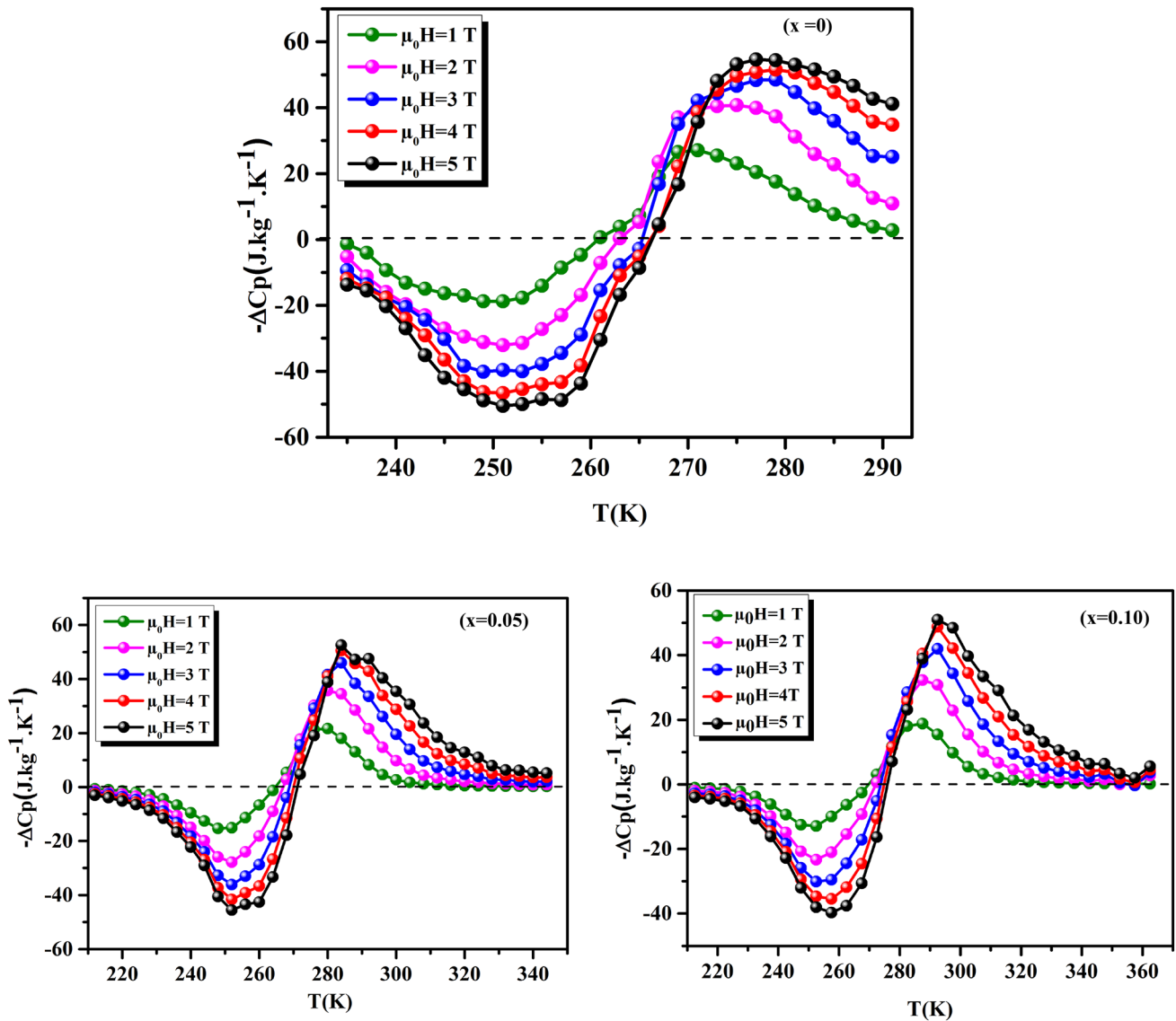


Fig. 9 $-\Delta C_p$ as function of temperatures for $\text{La}_{0.75}\text{Ca}_{0.25-x}\text{Na}_x\text{MnO}_3$ ($0 \leq x \leq 0.10$) samples at different magnetic fields

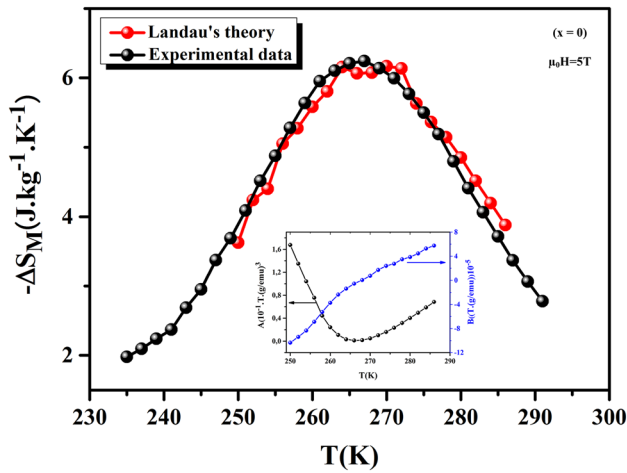


Fig. 10 Experimental and calculated values of $-\Delta S_M$ as function of temperatures, under 5 T magnetic field for $x=0$. The inset shows the Landau's coefficients $A(T)$ and $B(T)$

$$\begin{aligned} \Delta S_M(T, \mu_0 H) &= S_M(T, 0) - S_M(T, \mu_0 H) \\ &= -\frac{1}{2} \frac{\partial A}{\partial T} (M_0^2 - M^2) - \frac{1}{4} \frac{\partial B}{\partial T} (M_0^4 - M^4) \\ &\quad - \frac{1}{6} \frac{\partial C}{\partial T} (M_0^6 - M^6). \end{aligned} \tag{18}$$

The value of M_0 can be obtained by extrapolating M in the absence of a magnetic field. Figure 10 displays the variation of $-\Delta S_M$ as a function of temperatures under an applied magnetic field of 5 T, for $x=0$ as an example. We can see that the theoretical and experimental curves are in good agreement, which suggests that the present model does not take into account the influence of the Jahn–Teller's effect and exchange interactions on the magnetic properties of manganites [82].

3.5 Universal curve scaling analysis

Recently, Franco et al. have proposed a phenomenological universal curve for the applied magnetic field dependence of $-\Delta S_M$ [83]. This is based on normalizing all $-\Delta S_M(T, \mu_0 H)$ curves by the following expression:

$$\Delta S' = \Delta S_M(T, \mu_0 H) / \Delta S_M^{\max}. \tag{19}$$

In addition, the temperature axis is differently rescaled above and below T_C , as expressed in:

$$\theta = \begin{cases} \frac{T - T_C}{T_C - T_{r1}} & T < T_C \\ \frac{T - T_C}{T_{r2} - T_C} & T > T_C \end{cases}, \tag{20}$$

where $T_{r1,2}$ are the temperatures of two reference points, corresponding to $-\Delta S_M^{\max} / 2$ ($T_{r1} < T_C$ and $T_{r2} > T_C$). Figure 11 shows the variation of $\Delta S'$ as a function of θ , under different magnetic fields, for $\text{La}_{0.75}\text{Ca}_{0.25-x}\text{Na}_x\text{MnO}_3$ ($0 \leq x \leq 0.10$) samples. We can see that all curves collapse on the same curve. This confirms the second-order phase transition for our samples [84].

On the other hand, the search for universal curves and scaling laws emerges in all fields of scientific research. We can see clearly that all the experimental curves collapse on one universal curve. The universal curve can be well fitted by Lorentz function:

$$\Delta S' = \frac{a}{b + (\theta - c)^2}. \tag{21}$$

Generally, a , b , and c are free parameters. Taking into account the asymmetry of the plots, we can use two different sets of constants such as for $T < T_C$ region, $a = 0.952 \pm 0.013$, $b = 0.954 \pm 0.011$, and $c = -0.043 \pm 0.007$. While, for $T > T_C$ state $a = 0.537 \pm 0.030$; $b = 0.539 \pm 0.031$; and $c = 0.208 \pm 0.019$, for $x=0$ as an example. According to Eq. 21, the different $-\Delta S_M^{\max}$, T_C , T_{r1} and T_{r2} values are obligatory to characterize $-\Delta S_M$. Once we have determined the parameters from the properties of these materials, we can determine $-\Delta S_M$ from $\Delta S'$.

According to Oesterreicher et al. [85], the variation of $-\Delta S_M$ as a function of temperatures under different magnetic fields, for the magnetic materials with second-order phase transition around their T_C , follows an exponent power law:

$$\Delta S_M(T, \mu_0 H) = a(T) (\mu_0 H)^n, \tag{22}$$

where n is the critical exponent of the magnetic transition, defined as [86]:

$$n(T, \mu_0 H) = \frac{d \ln (|\Delta S_M|)}{d \ln (\mu_0 H)}. \tag{23}$$

Figure 12 shows the variation of n as a function of temperatures, for $x=0$ sample as an example, under different applied fields. In the FM region, n is close to 1. Then, it increased to 2, in PM state. Moreover, it decreased moderately with increasing temperature and a minimum value around T_C . These results are observed in different magnetic materials [87-90].

4 Conclusion

To sum up, we chose to detect the effect of low Na content on the $\text{La}_{0.75}\text{Ca}_{0.25-x}\text{Na}_x\text{MnO}_3$ sample. We prepared $\text{La}_{0.75}\text{Ca}_{0.25-x}\text{Na}_x\text{MnO}_3$ ($0 \leq x \leq 0.10$) using the flux method.

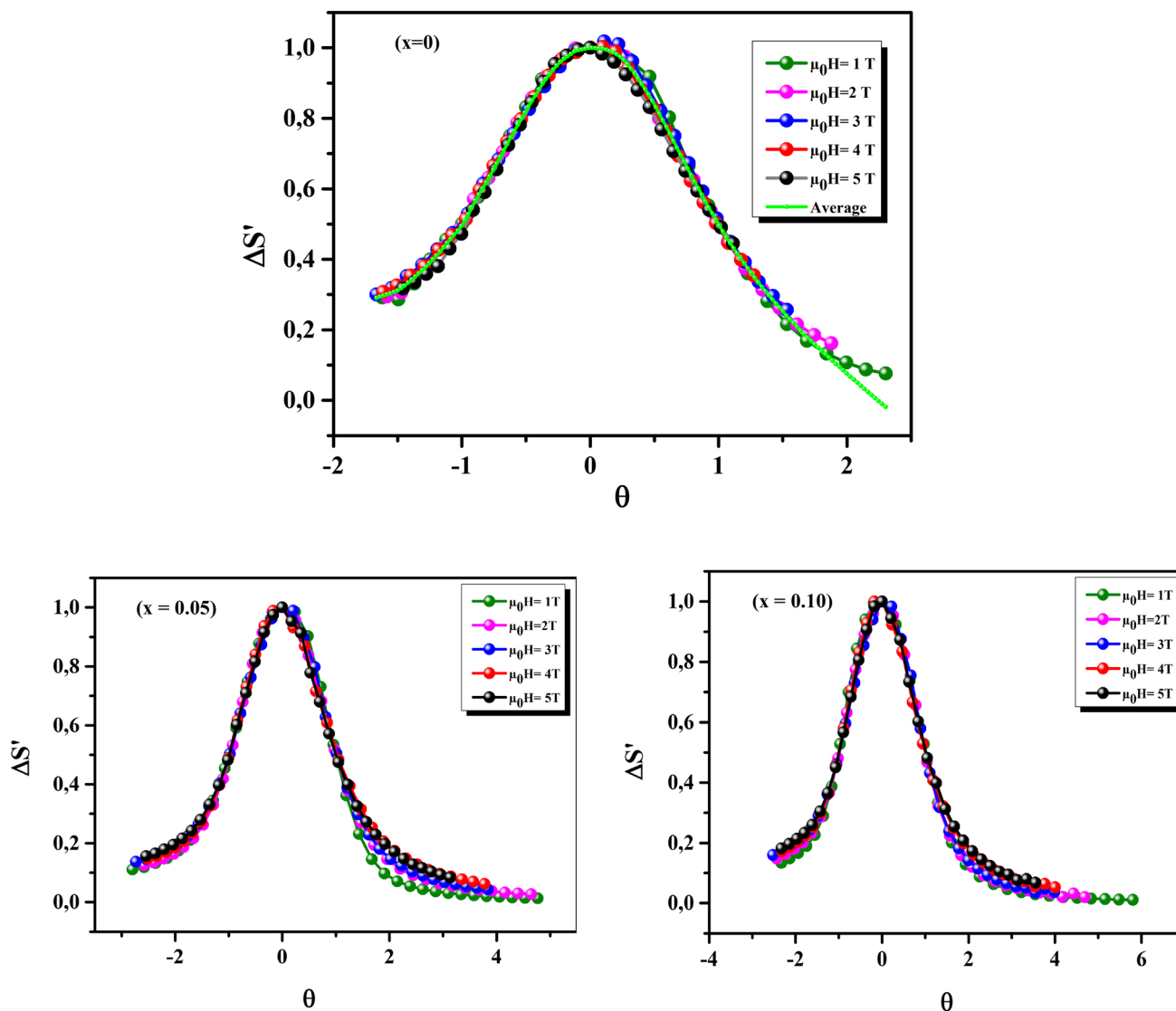


Fig. 11 Universal behavior of $\Delta S'(\theta)$ curves at different magnetic fields, for $\text{La}_{0.75}\text{Ca}_{0.25-x}\text{Na}_x\text{MnO}_3$ ($0 \leq x \leq 0.10$) samples

Then, we studied their structural and magnetic properties and MCE. Rietveld refinement of XRD patterns shows that our samples crystallize in an orthorhombic structure with a Pbnm space group, at room temperature. Substituting Ca^{2+} by Na^+ increased T_C from 268 to 278 K. This is accompanied by an increase of $-\Delta S_M$. Our samples have a second-order phase transition from FM to PM, upon increasing temperature. In addition, we found that $-\Delta S_M$ is in agreement with the theoretical one calculated using Landau's theory. From $x = 0.10$, the composition shows the largest value of $-\Delta S_M^{\text{max}} = 6.44 \text{ J kg}^{-1} \text{ K}^{-1}$ for $\mu_0 H = 5 \text{ T}$

in the series. Additionally, our samples exhibit high values of $\text{RCP} = 198, 270.5, \text{ and } 317.7 \text{ J k}^{-1}$ for $x = 0, 0.05, 0.10$, respectively. The magnetic entropy change was also characterized by one universal curve. This confirms that a second-order phase transition occurred. The obtained results indicate that $\text{La}_{0.75}\text{Ca}_{0.25-x}\text{Na}_x\text{MnO}_3$ ($0 \leq x \leq 0.10$) samples could be considered as a promising material for magnetic refrigeration technology. The most important results, in our present work, were compared with our last work for different doping rates of 0.15 and 0.20.

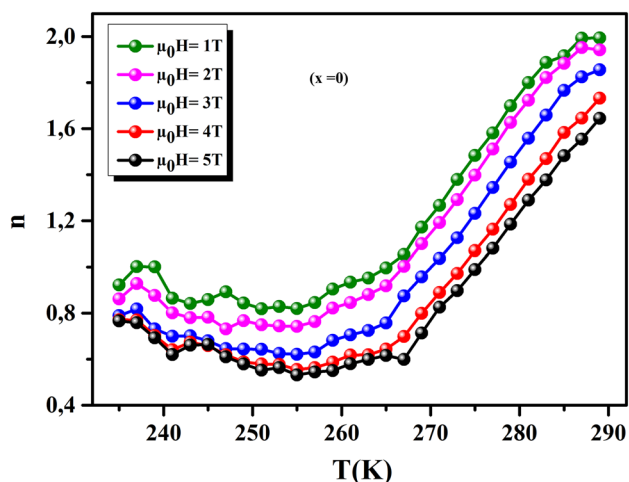


Fig. 12 Temperature dependence of local exponent n measured, at different magnetic fields, for $x=0$

References

1. K. Thanigai Arul, E. Manikandan, P.P. Murmu, J. Kennedy, M. Henini, Enhanced magnetic properties of polymer-magnetic nanostructures synthesized by ultrasonication. *J. Alloys Compd.* **720**, 395–400 (2017)
2. G.V.M. Williams, T. Prakash, J. Kennedy, S.V. Chong, S. Rubanov, Spin-dependent tunnelling in magnetite nanoparticles. *J. Magn. Magn. Mater.* **460**, 229–233 (2018)
3. T. Prakash, G.V.M. Williams, J. Kennedy, S. Rubanov, Formation of magnetic nanoparticles by low energy dual implantation of Ni and Fe into SiO_2 . *J. Alloys Compd.* **667**, 255–261 (2016)
4. X.S. Yang, L.Q. Yang, L. Lv, C.H. Cheng, Y. Zhao, Magnetic phase transition in $\text{La}_{0.7}\text{Sr}_{0.3}\text{MnO}_3/\text{Ta}_2\text{O}_5$ ceramic composites. *Ceram. Int.* **38**, 2575–2578 (2012)
5. T.-L. Phan, T.A. Ho, P.D. Thang, Q.T. Tran, T.D. Thanh, N.X. Phuc, M.H. Phan, B.T. Huy, S.C. Yu, Critical behavior of Y-doped $\text{Nd}_{0.7}\text{Sr}_{0.3}\text{MnO}_3$ manganites exhibiting the tricritical point and large magnetocaloric effect. *J. Alloys Compd.* **615**, 937 (2014)
6. T.A. Ho, T.L. Phan, P.D. Thang, S.C. Yu, Influence of Pb Doping on the Magnetocaloric Effect and Critical Behavior of $(\text{La}_{0.9}\text{Dy}_{0.1})_{0.8}\text{Pb}_{0.2}\text{MnO}_3$. *J. Electron. Mater.* **45**, 2328–2333 (2016)
7. M. Khelifi, M. Bejar, O. El Sadek, E. Dhahri, M.A. Ahmed, E.K. Hlil, Structural, magnetic and magnetocaloric properties of the lanthanum deficient in $\text{La}_{0.8}\text{Ca}_{0.2-x}\text{MnO}_3$ ($x=0-0.20$) manganites oxides. *J. Alloys Compd.* **509**, 7410–7415 (2011)
8. R.N. Mahato, K. Sethupathi, V. Sankaranarayanan, R. Nirmala, Large magnetic entropy change in nanocrystalline $\text{Pr}_{0.7}\text{Sr}_{0.3}\text{MnO}_3$. *J. Appl. Phys.* **107**, 09A943 (2010)
9. J. Khelifi, A. Tozri, F. Issaoui, E. Dhahri, E.K. Hlil, The influence of disorder on critical behavior near the paramagnetic to ferromagnetic phase transition temperature in $(\text{La}_{1-x}\text{Nd}_x)_2/3(\text{Ca}_{1-y}\text{Sr}_y)1/3\text{MnO}_3$ doped manganite. *J. Alloys Compd.* **584**, 6 (2014)
10. M. Khelifi, E. Dhahri, E.K. Hlil, Magnetic, magnetocaloric, magnetotransport and magnetoresistance properties of calcium deficient manganites $\text{La}_{0.8}\text{Ca}_{0.2-x}\text{MnO}_3$ post-annealed at 800°C . *J. Alloys Compd.* **587**, 771–777 (2014)
11. A.V. Trukhanov, M.A. Almessiere, A. Baykal, S.V. Trukhanov, Y. Slimani, D.A. Vinnik, V.E. Zhivulin, A.Yu. Starikov, D.S. Klygach, M.G. Vakhitov, T.I. Zubar, D.I. Tishkevich, E.L. Trukhanova, M. Zdorovets, Influence of the charge ordering and quantum effects in heterovalent substituted hexaferrites on their microwave characteristics. *J. Alloys Compd.* **788**, 1193–1202 (2019)
12. A.V. Trukhanov, M.A. Darwish, L.V. Panina, A.T. Morchenko, V.G. Kostishyn, V.A. Turchenko, D.A. Vinnik, E.L. Trukhanova, K.A. Astapovich, A.L. Kozlovskiy, M. Zdorovets, S.V. Trukhanov, Features of crystal and magnetic structure of the $\text{BaFe}_{12-x}\text{Ga}_x\text{O}_{19}$ ($x \leq 2$) in the wide temperature range. *J. Alloys Compd.* **791**, 522–529 (2019)
13. S.V. Trukhanov, A.V. Trukhanov, V.A. Turchenko, V.G. Kostishyn, L.V. Panina, I.S. Kazakevich, A.M. Balagurov, Structure and magnetic properties of $\text{BaFe}_{11.9}\text{In}_{0.1}\text{O}_{19}$ hexaferrite in a wide temperature range. *J. Alloys Compd.* **689**, 383–393 (2016)
14. A.V. Trukhanov, V.G. Kostishyn, L.V. Panina, S.H. Jabarov, V.V. Korovushkin, S.V. Trukhanov, E.L. Trukhanova, Magnetic properties and Mössbauer study of gallium doped M-type barium hexaferrites. *Ceram. Int.* **43**, 12822–12827 (2017)
15. I.O. Troyanchuk, S.V. Trukhanov, H. Szymczak, K. Baerner, Effect of oxygen content on the magnetic and transport properties of $\text{Pr}_{0.5}\text{Ba}_{0.5}\text{MnO}_{3-\gamma}$. *J. Phys. Condens. Matter* **12**, L155–L158 (2000)
16. S.V. Trukhanov, I.O. Troyanchuk, I.M. Fita, H. Szymczak, K. Bärner, Comparative study of the magnetic and electrical properties of $\text{Pr}_{1-x}\text{Ba}_x\text{MnO}_{3-\delta}$ manganites depending on the preparation conditions. *J. Magn. Magn. Mater.* **237**, 276–282 (2001)
17. S.V. Trukhanov, I.O. Troyanchuk, A.V. Trukhanov, I.M. Fita, A.N. Vasil'ev, A. Maignan, H. Szymczak, Magnetic properties of $\text{La}_{0.70}\text{Sr}_{0.30}\text{MnO}_{2.85}$ anion-deficient manganite under hydrostatic pressure. *JETP Lett.* **83**, 33–36 (2006)
18. G.H. Jonker, J.H. Van Santen, Ferromagnetic compounds of manganese with perovskite structure. *J. Phys.* **16** (1950), 337–349 (1950)
19. Y. Tokura, features of colossal magnetoresistive manganites. *Rep. Prog. Phys.* **69**, 797–851 (2006)
20. A.J. Millis, Lattice effects in magnetoresistive manganese perovskites. *Nature* **392**, 147–150 (1998)
21. A. Urushibara, Y. Moritomo, T. Arima, A. Asamitsu, G. Kido, Y. Tokura, Insulator-metal transition and giant magnetoresistance in $\text{La}_{1-x}\text{Sr}_x\text{MnO}_3$. *Phys. Rev. B* **51**, 14103–14109 (1995)
22. M. Itoh, T. Shimura, J.-D. Yu, T. Hayashi, Y. Inaguma, Structure dependence of the ferromagnetic transition temperature in rhombohedral $\text{La}_{1-x}\text{A}_x\text{MnO}_3$ ($\text{A}=\text{Na}, \text{K}, \text{Rb}, \text{and Sr}$). *Phys. Rev. B* **52**, 12522 (1995)
23. G.H. Rao, J.R. Sun, K. Barner, N. Hamad, Crystal structure and magnetoresistance of Na-doped LaMnO_3 . *J. Phys. Condens. Matter* **11**, 1523–1528 (1999)
24. I.O. Troyanchuk, S.V. Trukhanov, H. Szymczak, J. Przewoznik, K. Bärner, Phase transitions in $\text{La}_{1-x}\text{Ca}_x\text{MnO}_{3-x/2}$ manganites. *JETP* **9**, 161–167 (2001)
25. S.V. Trukhanov, N.V. Kasper, I.O. Troyanchuk, M. Tovar, H. Szymczak, K. Bärner, Evolution of magnetic state in the $\text{La}_{1-x}\text{Ca}_x\text{MnO}_{3-\gamma}$ ($x=0.30, 0.50$) manganites depending on the oxygen content. *J. Solid State Chem.* **169**, 85–95 (2002)
26. S.V. Trukhanov, L.S. Lobanovski, M.V. Bushinsky, V.A. Khomchenko, N.V. Pushkarev, I.O. Tyoyanchuk, A. Maignan, D. Flahaut, H. Szymczak, R. Szymczak, Influence of oxygen vacancies on the magnetic and electrical properties of $\text{La}_{1-x}\text{Sr}_x\text{MnO}_{3-x/2}$ manganites. *Eur. Phys. J. B* **42**, 51–61 (2004)
27. S.V. Trukhanov, Peculiarities of the magnetic state in the system $\text{La}_{0.70}\text{Sr}_{0.30}\text{MnO}_{3-\gamma}$ ($0 \leq \gamma \leq 0.25$). *JETP* **100**, 95–105 (2005)
28. S.G. TaoYi, X. Qi, Y. Zhu, F. Cheng, B. Ma, Y. Huang, C. Liao, C. Yan, Low temperature synthesis and magnetism of $\text{La}_{0.75}\text{Ca}_{0.25}\text{MnO}_3$ nanoparticles. *J. Phys. Chem. Solids* **61**, 1407–1413 (2000)

29. M. Pekala, V. Drozd, J. Mucha, Magnetic field dependence of electrical resistivity in fine grain La_{0.75}Ca_{0.25}MnO₃. *J. Magn. Mater.* **290–291**, 928–932 (2005)
30. Z.B. Guo, J.R. Zhang, H. Huang, W.P. Ding, Y.W. Du, Large magnetic entropy change in La_{0.75}Ca_{0.25}MnO₃. *Appl. Phys. Lett.* **70**, 904–905 (1997)
31. M.A. Almessiere, Y. Slimani, H. Güngüne, A. Bayka, S.V. Trukhanov, A.V. Trukhanov, Manganese/Yttrium codoped strontium nanohexaferrites: evaluation of magnetic susceptibility and Mössbauer spectra. *Nanomaterials* **9**, 24 (2019)
32. M.A. Almessiere, A.V. Trukhanov, Y. Slimani, K.Y. You, S.V. Trukhanov, E.L. Trukhanova, F. Esa, A. Sadaqat, K. Chaudhary, M. Zdorovets, A. Baykal, Correlation between composition and electrodynamic properties in nanocomposites based on hard/soft ferrimagnetics with strong exchange coupling. *Nanomaterials* **9**, 202–214 (2019)
33. S. Bouzidi, M.A. Gdaiem, J. Dhahri, E.K. Hlil, Large magnetocaloric entropy change at room temperature in soft ferromagnetic manganites. *RSC Adv* **9**, 65–76 (2019)
34. D.B. Wiles, R.A. Young, A new computer program for Rietveld analysis of X-ray powder diffraction patterns. *J. Appl. Crystallogr.* **14**, 149 (1981)
35. H.M. Rietveld, A profile refinement method for nuclear and magnetic structures. *J. Appl. Crystallogr.* **2**, 65–71 (1969)
36. L. Liu, H. Fan, S. Ke, X. Chen, Effect of sintering temperature on the structure and properties of cerium-doped 0.94 (Bi_{0.5}Na_{0.5})TiO₃-0.06 BaTiO₃ piezoelectric ceramics. *J. Alloys Compd.* **458**, 504–508 (2008)
37. Y.R. Zhang, J.F. Li, B.P. Zhang, Enhancing electrical properties in NBT-KBT lead-free piezoelectric ceramics by optimizing sintering temperature. *J. Am. Ceram. Soc.* **91**, 2716–2719 (2008)
38. Z. Wei, A. Chak-Tong, D.Y. Wei, Review of magnetocaloric effect in perovskite-type oxides. *Chin Phys B* **22**, 057501–057501–57511 (2013)
39. P. Schiffer, A.P. Ramirez, K.N. Franklin, S.-W. Cheon, Interaction-induced spin coplanarity in a kagomé magnet: SrCr₉Pd₁₂-9pO₁₉. *Phys. Rev. Lett.* **77**, 2085–2088 (1996)
40. H.L. Ju, H.C. Sohn, K.M. Krishnan, Evidence for O_{2p} hole-driven conductivity in La_{1-x}Sr_xMnO₃ (0 ≤ x ≤ 0.7) and La_{0.7}Sr_{0.3}MnO₃ thin films. *Phys. Rev. Lett.* **79**, 3230–3233 (1997)
41. R.D. Shannon, Revised effective ionic radii and systematic studies of interatomic distances in halides and chalcogenides. *Acta Crystallogr. A* **32**, 751–767 (1976)
42. K. Momma, F. Izumi, VESTA 3 for three-dimensional visualization of crystal, volumetric and morphology data. *J. Appl. Crystallogr.* **44**, 1272–1276 (2011)
43. A. Taylor, *X-Ray Metallography* (Wiley, New York, 1961)
44. W. Rasband, ImageJ, <https://rsb.info.nih.gov/ij/> (2005). Accessed Aug 2013
45. J. Gutiérrez, A. Peña, J.M. Barandiarán, J.L. Pizarro, T. Hernández, L. Lezama, M. Insausti, T. Rojo, Structural and magnetic properties of La_{0.7}Pb_{0.3}(Mn_{1-x}Fe_x)O₃ (0 ≤ x ≤ 0.3) giant magnetoresistance perovskites. *Phys. B* **61**, 9028–9035 (2000)
46. R. Mahesh, R. Mahendiran, A.K. Raychaudhuri, C.N.R. Rao, Effect of particle size on the giant magnetoresistance of La_{0.7}Ca_{0.3}MnO₃. *Appl. Phys. Lett.* **68**, 2291–2293 (1996)
47. V.D. Doroshev, V.A. Borodin, V.I. Kamenev, A.S. Mazur, T.N. Tarasenko, A.I. Tovstolytkin, S.V. Trukhanov, Self-doped lanthanum manganites as a phase-separated system: transformation of magnetic, resonance, and transport properties with doping and hydrostatic compression. *J. Appl. Phys.* **104**, 093909-1–093909-13 (2008)
48. N. Zhang, W. Ding, W. Zhong, D. Xing, Du Youwei, Tunnel-type giant magnetoresistance in the granular perovskite La_{0.85}Sr_{0.15}MnO₃. *Phys. Rev. B* **56**, 8138–8142 (1997)
49. D.N.H. Nam, R. Mathieu, P. Nordblad, N.V. Khiem, N.X. Phuc (2000) Ferromagnetism and frustration in Nd_{0.7}Sr_{0.3}MnO₃. *Phys. Rev. B* **62**:1027.
50. M.S. Kim, J.B. Yang, Q. Cai, X.D. Zhou, W.J. James, W.B. Yelon, P.E. Parris, D. Buddhikot, S.K. Malik, Structure, magnetic, and transport properties of Ti-substituted La_{0.7}Sr_{0.3}MnO₃. *Phys. Rev. B* **71**, 014433 (2005)
51. D.N.H. Nam, K. Jonason, P. Nordblad, N.V. Khiem, N.X. Phuc, Coexistence of ferromagnetic and glassy behavior in the La_{0.5}Sr_{0.5}CoO₃ perovskite compound. *Phys. Rev. B* **59**, 4189–4194 (1999)
52. W. Boujelben, A. Cheikh-Rouhou, J.C. Joubert, Ferromagnetism in lacunar perovskite manganites Pr_{0.7}Sr_{0.3-x}MnO₃ and Pr_{0.7-x}Sr_{0.3}MnO₃. *Eur. Phys. J. B.* **24**, 419–423 (2001)
53. L.Q. Zheng, Q.F. Fang, Magnetoresistance behavior in La_{0.7}Ca_xMnO₃ (x = 0.1–0.3) and La_yMnO₃ (y = 0.67–0.9) bulk materials. *Phys. Stat. Sol. (A)* **185**, 267–275 (2001)
54. A. Zaidi, K. Cherif, J. Dhahri, E.K. Hlil, M. Zaidi, T. Alharbi, Influence of Na-doping in La_{0.67}Pb_{0.33-x}Na_xMnO₃ (0 ≤ x ≤ 0.15) on its structural, magnetic and magneto-electrical properties. *J. Alloys Compd.* **650**, 210–216 (2015)
55. P.G. Radaelli, G. Iannone, M. Marezio, H.Y. Hwang, S.W. Cheong, J.D. Jorgensen, D.N. Argyriou, Structural effects on the magnetic and transport properties of perovskite A_{1-x}A'_xMnO₃ (x = 0.25, 0.30). *Phys. Rev. B* **56**, 8265–8282 (1997)
56. S.V. Trukhanov, Magnetic and magnetotransport properties of La_{1-x}Ba_xMnO_{3-x/2} perovskite manganites. *J. Mater. Chem.* **13**, 347–352 (2003)
57. S.V. Trukhanov, Investigation of Stability of Ordered Manganites. *JETP* **101**, 513–520 (2005)
58. C. Vázquez-Vázquez, M.A. López-Quintela, Solvothermal synthesis and characterisation of La_{1-x}A_xMnO₃ nanoparticles. *J. Solid State Chem.* **179**, 3229–3237 (2006)
59. C. Kittel, *Introduction to Solid State Physics*, 6th edn. (Wiley, New York, 1986)
60. A. Belkahlia, K. Cherif, J. Dhahri, K. Taibi, E.K. Hlil, Prediction of magnetoresistance using a magnetic field and correlation between the magnetic and electrical properties of La_{0.7}Bi_{0.05}Sr_{0.15}Ca_{0.1}Mn_{1-x}In_xO₃ (0 ≤ x ≤ 0.3) manganite. *RSC Adv.* **7**, 30707–30716 (2017)
61. Z.H. Wang, B.G. Shen, N. Tang, J.W. Cai, T. Hao Ji, J.G. Zhao, W.S. Zhan, Colossal magnetoresistance in cluster glass-like insulator La_{0.67}Sr_{0.33}(Mn_{0.8}Ni_{0.2})O₃. *J. Appl. Phys.* **85**, 5399–5401 (1999)
62. K. El Maalam, M. Ben Ali, H. El Moussaoui, O. Mounkachi, M. Hamedoun, R. Masrour, E.K. Hlil, A. Benyoussef, Magnetic properties of tin ferrites nanostructures doped with transition metal. *J. Alloys Compd.* **622**, 761–764 (2015)
63. B.K. Banerjee, On a generalised approach to first and second order magnetic transitions. *Phys. Lett.* **12**, 16–17 (1964)
64. L.E. Hueso, P. Sande, D.R. Miguens, J. Rivas, F. Rivadulla, M.A. Lopez-Quintela, Tuning of the magnetocaloric effect in La_{0.67}Ca_{0.33}MnO_{3-δ} nanoparticles synthesized by sol-gel techniques. *J. Appl. Phys.* **91**, 9943–9947 (2002)
65. W. Chen, W. Zheng, Y. Hou, R.W. Gao, W.C. Feng, M.G. Zhu, Y.Y. Du, Preparation and magnetocaloric effect of self-doped La_{0.8-x}Na_{0.2x}MnO_{3+δ} (= vacancies) polycrystal. *J. Phys. Condens. Matter* **14**, 11889–11896 (2002)
66. P. Sande, L.E. Hueso, D.R. Miguens, J. Rivas, F. Rivadulla, M.A. Lopez-Quintela, Large magnetocaloric effect in manganites with charge order. *J. Appl. Phys.* **79**, 2040–2042 (2001)
67. V. Karpasyuk, E. Beznisko, A. Abdullina, Generalized integro-differential equation of magnetization reversal dynamics in polycrystals and its application to processes in manganite-based CMR materials. *J. Magn. Magn. Mater.* **272–276**, 750–751 (2004)

68. R.D. Mc Michael, J.J. Ritter, R.D. Shull, Enhanced magnetocaloric effect in $Gd_3Ga_{5-x}Fe_xO_{12}$. *J. Appl. Phys.* **73**, 6946–6948 (1993)
69. H. Wada, Y. Tanabe, Giant magnetocaloric effect of $MnAs_{1-x}Sb_x$. *Appl. Phys. Lett.* **79**, 3302–3304 (2001)
70. A. Omri, M. Bejar, M. Sajieddine, E. Dhahri, E.K. Hlil, M. Es-Souni, Structural, magnetic and magnetocaloric properties of $AMn_{1-x}Ga_xO_3$ compounds with $0 \leq x \leq 0.2$. *Phys. B* **407**, 2566–2572 (2012)
71. A. Belkahl, K. Cherif, J. Dhahri, E.K. Hlil, large magnetic entropy change and magnetic field dependence of critical behavior studies in $La_{0.7}Bi_{0.05}Sr_{0.15}Ca_{0.1}Mn_{0.95}In_{0.05}O_3$ compound. *J. Alloys Compd.* **715**, 266–274 (2017)
72. K.A. Gschneidner Jr., V.K. Pecharsky, A.O. Tsokol, recent developments in magnetocaloric materials. *Rep. Prog. Phys.* **68**, 1479–1539 (2005)
73. J.S. Lee, Evaluation of the magnetocaloric effect from magnetization and heat capacity data. *Phys. State Solid B* **241**, 1765–1768 (2004)
74. K.A. Gschneidner Jr., V.K. Pecharsky, Magnetocaloric materials. *Rev. Mater. Sci.* **30**, 387–429 (2000)
75. H. Yang, Y.H. Zhu, T. Xian, J.L. Jiang, Synthesis and magnetocaloric properties of $La_{0.7}Ca_{0.3}MnO_3$ nanoparticles with different sizes. *J. Alloys Compd.* **555**, 150–155 (2013)
76. R. M'nassri, A. Cheikhrouhou, Magnetocaloric effect in different impurity doped $La_{0.67}Ca_{0.33}MnO_3$ composite. *J. Supercond. Nov. Magn.* **27**, 421–425 (2014)
77. V.S. Amaral, J.S. Amaral, Magnetoelastic coupling influence on the magnetocaloric effect in ferromagnetic materials. *J. Magn. Magn. Mater.* **272**, 2104–2105 (2004)
78. J.S. Amaral, M.S. Reis, V.S. Amaral, T.M. Mendonca, J.P. Araujo, M.A. Sa, P.B. Travers, J.M. Vieira, Magnetocaloric effect in Er- and Eu-substituted ferromagnetic La-Sr manganites. *J. Magn. Magn. Mater.* **290**, 686–689 (2005)
79. M.S. Anwar, S. Kumar, F. Ahmed, N. Arshi, G.W. Kim, B.H. Koo, Above room temperature magnetic transition and magnetocaloric effect in $La_{0.66}Sr_{0.34}MnO_3$. *J. Korean Phys. Soc.* **60**, 1587–1592 (2012)
80. M. Triki, R. Dhahri, M. Bekri, E. Dhahri, M.A. Valente, Magnetocaloric effect in composite structures based on ferromagnetic–ferroelectric $Pr_{0.6}Sr_{0.4}MnO_3/BaTiO_3$ perovskites. *J. Alloys Compd.* **509**, 9460–9465 (2011)
81. A. Tozri, E. Dhahri, E.K. Hlil, Magnetic transition and magnetic entropy changes of $La_{0.8}Pb_{0.1}MnO_3$ and $La_{0.8}Pb_{0.1}Na_{0.1}MnO_3$. *Mater. Lett.* **64**, 2138–2141 (2010)
82. R. M'nassri, W. Cheikhrouhou-Koubaa, N. Chniba-Boudjada, A. Cheikhrouhou, Effect of barium-deficiency on the structural, magnetic, and magnetocaloric properties of $La_{0.6}Sr_{0.2}Ba_{0.2-x}MnO_3$ ($0 \leq x \leq 0.15$). *J. Appl. Phys.* **113**, 073905 (2013)
83. V. Franco, J.S. Blázquez, A. Conde, Field dependence of the magnetocaloric effect in materials with a second order phase transition: a master curve for the magnetic entropy change. *Appl. Phys. Lett.* **89**, 222512 (2006)
84. Q.Y. Dong, H.W. Zhang, J.R. Sun, B.G. Shen, V. Franco, A phenomenological fitting curve for the magnetocaloric effect of materials with a second-order phase transition. *J. Appl. Phys.* **103**, 116101–116103 (2008)
85. H. Oesterreicher, F.T. Parker, Magnetic cooling near curie temperatures above 300 K. *J. Appl. Phys.* **55**, 4334–4338 (1984)
86. V. Franco, A. Conde, E.J.M. Romero, J.S. Blazquez, A universal curve for the magnetocaloric effect: an analysis based on scaling relations. *J. Phys. Condens. Matter* **20**, 285207–285211 (2008)
87. M. Pękala, Magnetic field dependence of magnetic entropy change in nanocrystalline and polycrystalline manganites $La_{1-x}M_xMnO_3$ ($M=Ca, Sr$). *J. Appl. Phys.* **108**, 113913–113916 (2010)
88. C.P. Reshmi, S. Savitha Pillai, M. Vasundhara, G.R. Raji, K.G. Suresh, M. Raama Varma, Co-existence of magnetocaloric effect and magnetoresistance in Co substituted $La_{0.67}Sr_{0.33}MnO_3$ at room temperature. *J. Appl. Phys.* **114**, 033904–033910 (2013)
89. V. Franco, C.F. Conde, J.S. Blazquez, A. Conde, P. Svec, D. Janičkovic, L.F. Kiss, A constant magnetocaloric response in FeMoCuB amorphous alloys with different FeB ratios. *J. Appl. Phys.* **101**, 093903–093911 (2007)
90. P. Nisha, S. Savitha Pillai, M. RaamaVarma, K.G. Suresh, Critical behavior and magnetocaloric effect in $La_{0.67}Ca_{0.33}Mn_{1-x}Cr_xO_3$ ($x=0.1, 0.25$). *Solid State Sci.* **14**, 40–47 (2012)
91. S.B. Tian, M.H. Phan, S.C. Yu, N.H. Hur, Magnetocaloric effect in a $La_{0.7}Ca_{0.3}MnO_3$ single crystal. *Phys. B* **327**, 221–224 (2003)
92. D.T. Morelli, A.M. Mance, J.V. Mantese, A.L. Micheli, Magnetocaloric properties of doped lanthanum manganite films. *J. Appl. Phys.* **79**, 373–375 (1996)
93. D.N.H. Nam, N.V. Dai, L.V. Hong, N.X. Phyc, S.C. Yu, M. Tachibana, E.T. Muromachi, Room-temperature magnetocaloric effect in $La_{0.7}Sr_{0.3}Mn_{1-x}M'_xO_3$ ($La_{0.7}Sr_{0.3}Mn_{1-x}M'_xO_3$ ($M'=Al, Ti$)). *J. Appl. Phys.* **103**, 043905–043909 (2008)
94. S. Ghodhbane, A. Dhahri, N. Dhahri, E.K. Hlil, J. Dhahri, Structural, magnetic and magnetocaloric properties of $La_{0.8}Ba_{0.2}Mn_{1-x}Fe_xO_3$ compounds with $0 \leq x \leq 0.1$. *J. Alloys Compd.* **550** (2013), 358–364 (2013)
95. K. Barik, C. Krishnamoorthi, R. Mahendiran, Effect of Fe substitution on magnetocaloric effect in $La_{0.7}Sr_{0.3}Mn_{1-x}Fe_xO_3$ ($0.05 \leq x \leq 0.20$). *J. Magn. Magn. Mater.* **323**, 1015–1021 (2011)

Publisher's Note Springer Nature remains neutral with regard to jurisdictional claims in published maps and institutional affiliations.